A subsynchronous resonance prevention for DFIG-based wind farms

Fateh, Davood; Birjandi, Ali Akbar MOTI; Guerrero, Josep M.

Published in:
Turkish Journal of Electrical Engineering and Computer Sciences

DOI (link to publication from Publisher):
10.3906/ELK-1912-177

Publication date:
2020

Document Version
Publisher's PDF, also known as Version of record

Turkish Journal of Electrical Engineering & Computer Sciences

http://journals.tubitak.gov.tr/elektrik/

Research Article

Turk J Elec Eng & Comp Sci
(2020) 28: 2670 – 2685

doi:10.3906/elk-1912-177

A subsynchronous resonance prevention for DFIG-based wind farms

Davood FATEH[1], **Ali Akbar MOTI BIRJANDI**[1,*], **Josep M. GUERRERO**[2]

[1]Department of Electrical Engineering, Faculty of Engineering, Shahid Rajaee Teacher Training University, Tehran, Iran

[2]The Villum Center for Research on Microgrids (CROM), Department of Energy Technology, Aalborg University, Aalborg, Denmark

Received: 11.01.2020 • **Accepted/Published Online:** 04.05.2020 • **Final Version:** 25.09.2020

Abstract: In this paper, subsynchronous resonance (SSR) instability was accurately analyzed in doubly fed induction generator (DFIG)-based wind farms by the linearization of equations and modal analysis. In addition, the possibility of high compensation for the transmission lines connected to DFIG-based wind farms was provided using a SSR prevention controller (SSRPC). For this purpose, an SSRPC was connected to the output voltage of the grid side converter (GSC) of the DFIG. The GSC output voltage was selected as the connection point of the SSRPC because it directly affects the induction generator effect (IGE) and can be an inhibitor factor in its occurrence. Furthermore, using system dynamic equations and the participation factor, it was shown that the effective factor on subsynchronous mode was the capacitor series voltage of the line, considered an input signal to the SSRPC. To validate the performance of the proposed method, a simulation was performed based on the IEEE SSR first benchmark model using the software MATLAB/Simulink.

Key words: SSR, DFIG-based wind farm, SSR prevention controller, line series capacitor voltage

1. Introduction

Today, with the extensive growth of wind farms, the maximum transmission of their production power is a major issue in power systems. Among the methods for increasing the transmission power of the lines, the use of capacitive series compensation is the most economical. However, the compensation level of the transmission lines connected to doubly fed induction generator (DFIG)-based wind farms is not sufficiently high. In this regard, if the DFIG-based wind farm becomes in series with the capacitive series compensated transmission line, the probability of the subsynchronous resonance (SSR) phenomenon occurring will increase due to the high inductive properties of DFIGs. The SSR phenomenon occurs under the two following conditions: the induction generator effect (IGE) and torsional interactions (TIs). TIs rarely occur in DFIG-based wind farms due to the low shaft stiffness of the wind turbine, and the main reason for the occurrence of SSR is the IGE. Owing to the possible occurrence of the SSR phenomenon in DFIG-based wind farms, the compensation level is not high. In this respect, for the first time, the Texas Public Utility Commission used a transmission line with 50% compensation level to transmit the wind farm power in western Texas in 2005. In addition, in the south of Minnesota, a transmission line with 60% compensation was used to transfer the electrical power of a 150-MW DFIG-based wind farm. In 2009, a DFIG-based wind farm of the Texas Electric Reliability Association was radially placed with a capacitive compensated transmission line, and the first SSR occurred in DFIG-based wind farms [1–5].

*Correspondence: Motiebirjandi@sru.ac.ir

After 2009, studies began to focus on the SSR phenomenon and its mitigation in DFIG-based wind farms. For instance, authors used the SVC to mitigate SSR in DFIG-based wind farms [6–9]. In another study [7], one controller with a simple gain was utilized as the damping controller, and the line real power was considered as the input signal to this controller. In Varma et al. [9], the impact of a static var compensator (SVC) and a thyristor-controlled series capacitor (TCSC) was examined on SSR. Mohammadpour and Santi [10] presented the ability of a TCSC to damp the IGE. Moreover, other authors [10, 12] used a gate-controlled series capacitor (GCSC) to mitigate the SSR in DFIG-based wind farms. A controller called an SSR damping controller (SSRDC) was used to control the GCSC. In addition, the impact of static series synchronous compensation (SSSC) on SSR mitigation was studied [13, 14]. Moreover, the use of STATCOM for SSR mitigation in SEIG-based wind farms was further considered in other studies [11, 14–17], where various controllers were hired for this equipment.

The use of FACTS devices and their controllers possibly causes subsynchronous control interactions (SSCIs). Furthermore, FACTS devices are cost effective and produce harmonics. In contrast, DFIG converters, while functioning similarly, do not have the problems of FACTS devices. For these reasons, DFIG converters are preferable for mitigating SSR. In previous research [18, 19], the GSC of DFIG-based wind farms was employed to mitigate SSR. In these articles, SSR was mitigated using the reference voltages of the GSC. Zhao et al. [20] used a rotor side converter (RSC) to control active power and mitigate the SSR in DFIG-based wind farms. Furthermore, in Mohammadpour and Santi [21], both GSC and RSC converters were employed to mitigate SSR. However, in these studies, the maximum power point tracking (MPPT) conditions were not maintained.

In other work [22–25], methods were presented to mitigate the SSCI as a new type of SSR. In addition, other authors [26–28] studied the SSR in DFIG-based wind farms. Chen et al. [29] proposed a piecewise probabilistic collocation method to assess the probabilistic stability of SSR. Other methods have been further devised to mitigate SSR. For instance, in Xie et al. [30], the series capacitor was removed at the time of SSR occurrence. Elsewhere [31, 32], the blocking filter (BF) set at the natural frequency of the generator turbine shaft was utilized to mitigate the TI type of SSR. However, this filter is not suitable for SSR mitigation in DFIG-based wind farms. In other research [31–34], the authors used a bypass filter parallel to a line series capacitor, with the filter set at the main frequency of the system. This series filter is suitable for mitigating SSR due to IGE in DFIG-based wind farms. Additionally, in a costly method a subsynchronous frequency relay and a damper winding were used to mitigate SSR [31, 32, 35, 36]. Bongiorno and Petersson [37] indicated that SSR could be avoided by selecting different compensation levels, which is an impossible task.

To enhance the power transfer capacity of the line, the compensation level has to be increased. In addition, at high compensation levels, SSR instability is likely to occur. To prevent this phenomenon, this paper presents its accurate analysis using the full equations of a standard system. Furthermore, a method using the SSRPC and GSC output voltage was employed to increase the capacitive series compensation level of the lines connected to DFIG-based wind farms. For this purpose, a SSR prevention controller (SSRPC) was proposed and connected to the output voltage of the GSC. Furthermore, the GSC output voltage was selected as input signal to the SSRPC because it has a direct effect on the line current and can be a deterrent factor in IGE. Moreover, GSC output voltage was selected owing to the maintenance of MPPT conditions, which has not been mentioned in previous work. Using this method, MPPT was maintained since the output voltage of the GSC has no direct effect on the turbine speed, power, or torque. Additionally, the dynamic equations of the system were fully described; with the linearization of the equations and modal analysis, the SSR mode was detected and the system instability conditions were investigated. Selection of the input signal to the proposed

controller was based on the participation coefficient, a highly effective method for detecting the state variable that is more effective on SSR mode. The IEEE SSR first benchmark model was employed to simulate and show the accuracy of the results in the software MATLAB/Simulink. The results showed that this study provided the possibility of high compensation in the line connected to DFIG-based wind farms, particularly wind farms in areas with low wind speed.

2. Modeling of the system

Figure 1 shows the IEEE SSR first benchmark model. The system includes a wind farm connected to a capacitive series compensated line, and the line end is an infinite bus. Because the parameters of a wind farm are equivalent to those of a DFIG, the DFIGs of a wind farm can be modeled by an equivalent DFIG [38–41]. In this regard, only the power of the wind farm is equal to the DFIGs' total power. For instance, a wind farm composed of 50 DFIGs with 2-MW power can be modeled as a 100-MW generator [42]. With this selection, MPPT is maintained, which has not been considered previously.

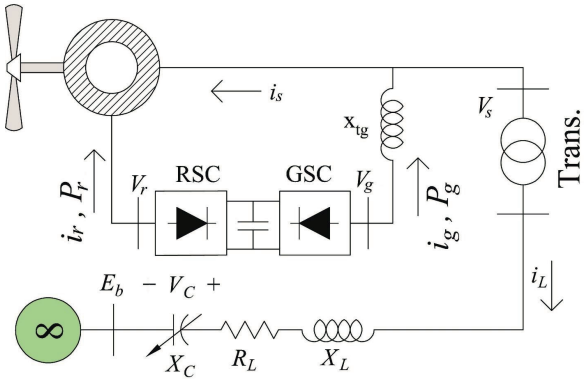

Figure 1. IEEE SSR first benchmark model.

To analyze this system dynamically, it is necessary to study its differential and algebraic equations.

2.1. Induction generator equations in qd0-frame

Differential equations of the induction generator are shown in Eqs. (1)–(4) [43].

$$\dot{\psi}_{qs} = \omega_b.v_{qs} - \omega_b.R_s.i_{qs} - \omega.\psi_{ds} \tag{1}$$

$$\dot{\psi}_{ds} = \omega_b.v_{ds} - \omega_b.R_s.i_{ds} + \omega.\psi_{ds} \tag{2}$$

$$\dot{\psi}_{qr} = \omega_b.v_{qr} - \omega_b.R_r.i_{qr} - (\omega - \omega_r).\psi_{dr} \tag{3}$$

$$\dot{\psi}_{dr} = \omega_b.v_{dr} - \omega_b.R_r.i_{dr} + (\omega - \omega_r).\psi_{qr} \tag{4}$$

The algebraic equations of the induction generators are also shown as follows [43]:

$$i_{qs} = \frac{X_{rr}}{D}.\psi_{qs} - \frac{X_M}{D}.\psi_{qr} \tag{5}$$

$$i_{ds} = \frac{X_{rr}}{D}.\psi_{ds} - \frac{X_M}{D}.\psi_{dr} \tag{6}$$

$$i_{qr} = -\frac{X_M}{D}.\psi_{qs} + \frac{X_{ss}}{D}.\psi_{qr} \tag{7}$$

$$i_{dr} = -\frac{X_M}{D}.\psi_{ds} + \frac{X_{ss}}{D}.\psi_{dr}, \tag{8}$$

where ψ_{qs}, ψ_{ds}, ψ_{qr}, and ψ_{dr} are flux linkages per second of stator and in the qd0-frame, respectively. v_{qs}, v_{ds}, v_{qr}, and v_{dr} are the stator's and rotor's voltages in the qd0-frame, respectively. i_{qs}, i_{ds}, i_{qr}, and i_{dr} are the stator's and rotor's currents in the qd0-frame, respectively. ω_b is base frequency and is equal to the synchronous frequency. ω is the qd0-frame rotating speed and is equal to the base frequency in the present paper. R_s and R_r are the stator's resistance and the rotor's resistance, respectively. X_{ls}, X_{lr}, and X_M are stator leakage reactance, rotor leakage reactance, and magnetic reactance, respectively. Moreover, $X_{ss} = X_{ls} + X_M$ and $X_{rr} = X_{lr} + X_M$. All of these parameters are in the per-unit system (pu).

2.2. Rotor shaft equations

In order to study SSR, the wind turbine shaft is modeled with two masses. One of the masses is related to a turbine shaft with low speed and another mass is related to a generator rotor shaft with high speed. Their differential equations are shown as follows [42]:

$$\dot{\omega}_t = \frac{-D_t - D_{tg}}{2H_t}.\omega_t + \frac{D_{tg}}{2H_t}.\omega_r - \frac{1}{2H_t}.T_g + \frac{1}{2H_t}.T_{wind} \tag{9}$$

$$\dot{\omega}_r = \frac{D_{tg}}{2H_g}.\omega_t + \frac{-D_g - D_{tg}}{2H_g}.\omega_r + \frac{1}{2H_g}.T_g - \frac{1}{2H_g}.T_e \tag{10}$$

$$\dot{T}_g = K_{tg}.\omega.\omega_t - K_{tg}.\omega.\omega_r, \tag{11}$$

where ω_t, ω_r, and T_g are the wind turbine speed, the rotor speed, and the torque between two masses, respectively. T_{wind} and T_e are the wind torque and the generator's electrical torque, respectively. All of these parameters are in pu. The electric torque is also calculated from Eq. (12). To obtain the MPPT, the reference electric torque is determined by a lookup table (Table 1). In this table, in order to extract the maximum power of the turbine, there are optimal rotor speed, wind power, and wind torque for each wind speed. Based on this table, for each wind speed, the reference value of electric torque is selected and applied to the RSC controller.

$$T_e = 0.5X_M.(i_{qs}.i_{dr} - i_{ds}.i_{qr}) \tag{12}$$

2.3. DFIG converter controllers and DC-link capacitor

The DFIG consists of two converters as shown in Figure 1: the grid side converter (GSC) and the rotor side converter (RSC). The DFIG converters adjust the generator terminal and the rotor voltages. To control these converters, the controllers shown in Figures 2a and 2b were used. Previous reports [44, 45] stated that the torque and the q-axis component of the rotor voltage are related. The reactive power and the d-axis component

of the rotor voltage are also related. On the other hand, the torque is proportional to the q-axis component of the rotor current and the reactive power is proportional to the d-component of the rotor current. Accordingly, the RSC controller is designed. The basis of the design of the GSC controller is the same. The reference torque was selected and applied to the RSC controller based on the wind speed and the lookup table. Additionally, the dynamic of the DC-link capacitor between the DFIG converters was modeled as a first-order equation by Eqs. (13)–(15) [42].

$$c.V_{DC}.\frac{dV_{DC}}{dt} = -(P_r + P_g) \tag{13}$$

$$P_r = 0.5(v_{qr}.i_{qr} + v_{dr}.i_{dr}) \tag{14}$$

$$P_g = 0.5(v_{qg}.i_{qg} + v_{dg}.i_{dg}), \tag{15}$$

where P_r and P_g are the RSC and the GSC output active powers, respectively, and c is the DC-link capacitor. Figure 2c shows the power distribution between the RSC, the GSC, and the DC-link capacitor.

Table 1. MPPT lookup table.

V_w(m/s)	7	8	9	10	11	12
ω_r(pu)	0.75	0.85	0.95	1.05	1.15	1.25
P_{wind}(pu)	0.32	0.49	0.69	0.95	1.25	1.6
T_{wind}=P_{wind}/ω_r	0.43	0.58	0.73	0.90	1.09	1.28

The stator output reactive power is calculated by Eq. (16).

$$Q_s = 0.5(v_{qs}.i_{ds} - v_{ds}.i_{qs}) \tag{16}$$

The GSC output is connected to the generator stator output terminal by a transformer. Eqs. (17)–(20) are obtained by Kirchhoff's voltage law (KVL) and Kirchhoff's current law (KCL). These equations present the algebraic equations between the GSC output and the stator output terminal.

$$v_{qg} = v_{qs} + X_{tg}.i_{dg} \tag{17}$$

$$v_{dg} = v_{ds} - X_{tg}.i_{qg} \tag{18}$$

$$i_{qg} = i_{qs} + I_{qL} \tag{19}$$

$$i_{dg} = i_{ds} + I_{dL}, \tag{20}$$

where v_{qg} and v_{dg} are the output voltage of the GSC in the qd0-frame, respectively. i_{qg} and v_{dg} are the output current of the GSC in the qd0-frame, respectively. I_{qL} and I_{dL} are the line currents in the qd0-frame, respectively. X_{tg} is the transformer impedance.

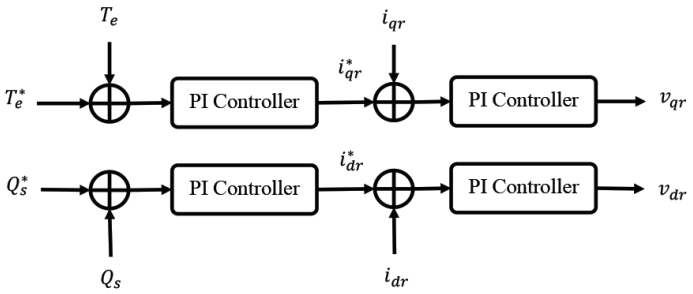

(a) RSC controller

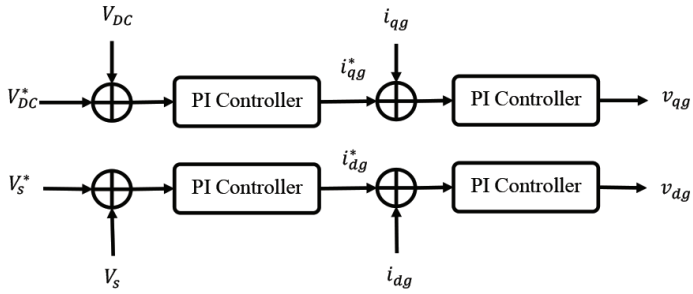

(b) GSC controller

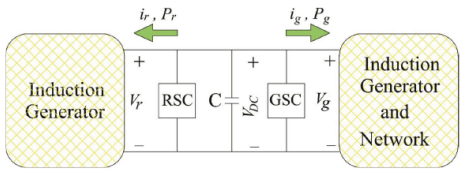

(c) Power distribution between RSC, GSC, and DC-link capacitor

Figure 2. DFIG converter controllers.

2.4. Differential equations of the capacitive series-compensated line

The differential equations of the transmission line and its capacitors are presented as follows [42]:

$$\dot{I}_{qL} = -\frac{R_L}{X_L}.\omega_b.I_{qL} - \omega.I_{dL} - \frac{\omega_b}{X_L}.v_{qc} + \frac{\omega_b}{X_L}.v_{qs} - \frac{\omega_b}{X_L}.E_{qB} \tag{21}$$

$$\dot{I}_{dL} = \omega.I_{qL} - \frac{R_L}{X_L}.\omega_b.I_{dL} - \frac{\omega_b}{X_L}.v_{dc} + \frac{\omega_b}{X_L}.v_{ds} - \frac{\omega_b}{X_L}.E_{dB} \tag{22}$$

$$\dot{v}_{qc} = \omega_b.X_c.I_{qL} - \omega.v_{dc} \tag{23}$$

$$\dot{v}_{dc} = \omega_b.X_c.I_{dL} + \omega.v_{qc}, \tag{24}$$

where v_{qc} and v_{dc} are the series capacitor voltages in qd0-frame, respectively. I_{qL} and I_{dL} are the line currents in the qd0-frame, respectively. v_{qs}, v_{ds}, E_{qB}, and E_{dB} are the stator and the infinite bus voltages in the qd0-frame, respectively. All of these parameters except ω and ω_b are in pu.

3. SSR definition

The SSR phenomenon is the condition in which the wind plant exchanges in one or more natural frequencies with the electric network. In a power system with the capacitive series compensation, the network has a natural frequency that is calculated as follows: $f_n = f_s\sqrt{X_c/X_L}$, where f_n and f_s are the natural frequency (Hz) and the synchronous frequency (Hz), respectively. X_L is the line reactance, in pu, and X_c is the series capacitor reactance of the line. It is the percentage of the line reactance, which is called the compensation percentage (K %). According to f_n, slip s_n is introduced as follows [12, 42, 46, 47]:

$$s_n = \frac{f_n - f_r}{f_n}, \tag{25}$$

where f_r is the rotor electrical frequency (Hz). As the f_n is lower than the f_r, then the s_n is negative. Therefore, the rotor equivalent resistance is negative in the subsynchronous frequency. In other words, $R_{r,eq} = R_r/s_n$ is negative. If the amplitude of this resistance increases from the total resistances of the network and generator armature, then the total resistance of the system (R_{sys}) will be negative at the subsynchronous frequency. Thus, according to Eq. (26), the second part of the total current of the system will have an exponential function with positive power. Therefore, the line current increases exponentially and this phenomenon is called the IGE.

In addition, a component with the resonant frequency (f_n) appears in the stator current and complementary frequency $(f_s - f_n)$ of this component appears in the rotor current. The TI happens when the torsional mode frequency between the rotor masses is close and coincides with this complementary frequency. Since the rotor shaft stiffness of the wind turbines is low, their torsional mode frequency is also low. For this reason, the SSR rarely occurs due to the TI in the wind power plants, because the torsional mode frequency in wind power plants is about 1–3 Hz. Therefore, the TI occurs when the resonant frequency is between 57 and 59 Hz, which requires a very high compensation level. Thus, its probability is very low [42].

$$i = A.\sin(2\pi f_s.t) + e^{-(\frac{R_{sys}}{L}).t}.B.\sin(2\pi f_n.t + \theta) \tag{26}$$

To detect the SSR mode, the system has to be dynamically analyzed. In addition, the instability conditions of this mode should be studied. Using the modal analysis and computing the participation factors, the effective input signal was then detected in the proposed controller. It should be noted that the participation factor represents a criterion of the relative participation of the state variable i in the kth mode and is defined as (27) [48, 49].

$$P_{ik} = v_{ik}.u_{ki}, \tag{27}$$

where v_{ik} and u_{ki} are the element-i of the k^{th} mode right eigenvector and the element-i of the k^{th} mode left eigenvector, respectively.

4. System dynamics analysis

To analyze the system dynamically, the system equations need to be linearized around the operating point. With the linearization of the system differential equations, Eqs. (28)–(39) are obtained.

$$\Delta\dot{\psi}_{qs} = \omega_b.\Delta v_{qs} - \omega_b.R_s.\Delta i_{qs} - \omega.\Delta\psi_{ds} \tag{28}$$

$$\Delta\dot{\psi}_{ds} = \omega_b.\Delta v_{ds} - \omega_b.R_s.\Delta i_{ds} + \omega.\Delta\psi_{qs} \tag{29}$$

$$\Delta\dot{\psi}_{qr} = \omega_b.\Delta v_{qr} - \omega_b.R_r.\Delta i_{qr} - (\omega - \omega_{ro}).\Delta\psi_{dr} + \psi_{dro}.\Delta\omega_r \tag{30}$$

$$\Delta\dot{\psi}_{dr} = \omega_b.\Delta v_{dr} - \omega_b.R_r.\Delta i_{dr} + (\omega - \omega_{ro}).\Delta\psi_{qr} - \psi_{qro}.\Delta\omega_r \tag{31}$$

$$\Delta\dot{\omega}_t = \frac{-D_t - D_{tg}}{2H_t}.\Delta\omega_t + \frac{D_{tg}}{2H_t}.\Delta\omega_r - \frac{1}{2H_t}.\Delta T_g + \frac{1}{2H_t}.\Delta T_{wind} \tag{32}$$

$$\Delta\dot{\omega}_r = \frac{D_{tg}}{2H_g}.\Delta\omega_t + \frac{-D_g - D_{tg}}{2H_g}.\Delta\omega_r + \frac{1}{2H_g}.\Delta T_g - \frac{1}{2H_g}.\Delta T_e \tag{33}$$

$$\Delta\dot{T}_g = K_{tg}.\omega.\Delta\omega_t - K_{tg}.\omega.\Delta\omega_r \tag{34}$$

$$\Delta\dot{I}_{qL} = -\frac{R_L}{X_L}.\omega_b.\Delta I_{qL} - \omega.\Delta I_{dL} - \frac{\omega_b}{X_L}.\Delta v_{qc} + \frac{\omega_b}{X_L}.\Delta v_{qs} - \frac{\omega_b}{X_L}.\Delta E_{qB} \tag{35}$$

$$\Delta\dot{I}_{dL} = \omega.\Delta I_{qL} - \frac{R_L}{X_L}.\omega_b.\Delta I_{dL} - \frac{\omega_b}{X_L}.\Delta v_{dc} + \frac{\omega_b}{X_L}.\Delta v_{ds} - \frac{\omega_b}{X_L}.\Delta E_{dB} \tag{36}$$

$$\Delta\dot{v}_{qc} = \omega_b.X_c.\Delta I_{qL} - \omega.\Delta v_{dc} \tag{37}$$

$$\Delta\dot{v}_{dc} = \omega_b.X_c.\Delta I_{dL} + \omega.\Delta v_{qc} \tag{38}$$

$$\Delta\dot{v}_{DC} = -\frac{1}{c}[\frac{(P_{ro} + P_{go})}{-v_{DCo}^2}\Delta v_{DC} + \frac{1}{v_{DCo}}(\Delta P_r + \Delta P_g)] \tag{39}$$

Furthermore, with the linearization of the system algebraic equations, Eqs. (40)–(51) are obtained:

$$\Delta i_{qs} = \frac{X_{rr}}{D}.\Delta\psi_{qs} - \frac{X_M}{D}.\Delta\psi_{qr} \tag{40}$$

$$\Delta i_{ds} = \frac{X_{rr}}{D}.\Delta\psi_{ds} - \frac{X_M}{D}.\Delta\psi_{dr} \tag{41}$$

$$\Delta i_{qr} = -\frac{X_M}{D}.\Delta\psi_{qs} + \frac{X_{ss}}{D}.\Delta\psi_{qr} \tag{42}$$

$$\Delta i_{dr} = -\frac{X_M}{D}.\Delta\psi_{ds} + \frac{X_{ss}}{D}.\Delta\psi_{dr} \tag{43}$$

$$\Delta v_{qg} = \Delta v_{qs} + X_{tg}.\Delta i_{dg} \tag{44}$$

$$\Delta v_{dg} = \Delta v_{ds} - X_{tg}.\Delta i_{qg} \tag{45}$$

$$\Delta i_{qg} = \Delta i_{qs} + \Delta I_{qL} \tag{46}$$

$$\Delta i_{dg} = \Delta i_{ds} + \Delta I_{dL} \tag{47}$$

$$\Delta T_e = 0.5X_M.(i_{qso}.\Delta i_{dr} + i_{dro}.\Delta i_{qs} - i_{dso}.\Delta i_{qr} - i_{qro}.\Delta i_{ds}) \tag{48}$$

$$\Delta P_r = 0.5(v_{qro}.\Delta i_{qr} + i_{qro}.\Delta v_{qr} + v_{dro}.\Delta i_{dr} + i_{dro}.\Delta v_{dr}) \tag{49}$$

$$\Delta P_g = 0.5(v_{qgo}.\Delta i_{qg} + i_{qgo}.\Delta v_{qg} + v_{dgo}.\Delta i_{dg} + i_{dgo}.\Delta v_{dg}) \tag{50}$$

$$\Delta Q_s = 0.5(v_{qso}.\Delta i_{ds} + i_{dso}.\Delta v_{qs} - v_{dso}.\Delta i_{qs} - i_{qso}.\Delta v_{ds}), \tag{51}$$

where if the following vectors are defined:

$$\Delta\psi = \begin{bmatrix}\Delta\psi_{qs}\\ \Delta\psi_{ds}\\ \Delta\psi_{qr}\\ \Delta\psi_{dr}\end{bmatrix},\ \Delta\Omega = \begin{bmatrix}\Delta\omega_t\\ \Delta\omega_r\\ \Delta T_g\end{bmatrix},\ \Delta I_L = \begin{bmatrix}\Delta I_{qL}\\ \Delta I_{dL}\\ \Delta v_{qc}\\ \Delta v_{dc}\end{bmatrix},\ \Delta I = \begin{bmatrix}\Delta i_{qs}\\ \Delta i_{ds}\\ \Delta i_{qr}\\ \Delta i_{dr}\end{bmatrix},\ \Delta v_s = \begin{bmatrix}\Delta v_{qs}\\ \Delta v_{ds}\end{bmatrix},$$

$$\Delta v_r = \begin{bmatrix}\Delta v_{qr}\\ \Delta v_{ds}\end{bmatrix},\ \Delta v_g = \begin{bmatrix}\Delta v_{qg}\\ \Delta v_{dg}\end{bmatrix},\ \Delta I_g = \begin{bmatrix}\Delta i_{qg}\\ \Delta i_{dg}\end{bmatrix},\ \Delta u = \begin{bmatrix}\Delta T_{wind}\\ \Delta E_{qB}\\ \Delta E_{dB}\end{bmatrix}$$

To analyze the modal, it is necessary to eliminate the algebraic relations to obtain the system state matrix. For this purpose, the RSC voltage vector (Δv_r) and the GSC voltage vector (Δv_g) are selected as the system control inputs, and the stator voltage vector (Δv_s) is deleted. Therefore, (52) is obtained.

$$\Delta\dot{X} = A_{sys}.\Delta X + B_{Con}.\Delta V + E.\Delta u, \tag{52}$$

where ΔX is the vector of state variables and contains the vectors $\Delta\psi$, $\Delta\Omega$, ΔI_L, and Δv_{DC}. ΔV is the control inputs vector and contains Δv_r and Δv_g. A_{sys}, B_{Con}, and E are the system state matrix, the system control inputs matrix, and the system input matrix, respectively. By obtaining the system poles using the matrix A_{sys}, the SSR mode is obtained with a frequency lower than the synchronous frequency.

5. SSR prevention controller (SSRPC)

The SSR prevention controller (SSRPC) is connected to the d-axis output voltage of the GSC. The reason behind selecting the GSC output voltage is to prevent the IGE and maintain MPPT. According to the line current equations, the stator voltage directly affects the line current. In addition, the stator voltage is controlled by v_{dg} of the GSC. Therefore, v_{dg} can be a deterrent factor in the IGE that does not directly affect MPPT parameters such as the turbine speed, power, or torque. Because in this part of the GSC there is no feedback from the turbine speed, power, or torque, there will not be any significant changes in MPPT conditions. Nevertheless, the SSRPC does not apply to the reference voltage (v_S^*) or the reference current (I_{dg}^*) since by applying SSRPC to the stator reference voltage (v_S^*) or the GSC controller reference current (I_{dg}^*), a change is generated in the reference value of the stator voltage or current, significantly increasing the steady state values of the stator voltage and the line current. However, by applying the SSRPC to Δv_{dg}, their steady state values do not increase. Figure 3 shows the connection point SSRPC. This controller includes a PI controller and a filter.

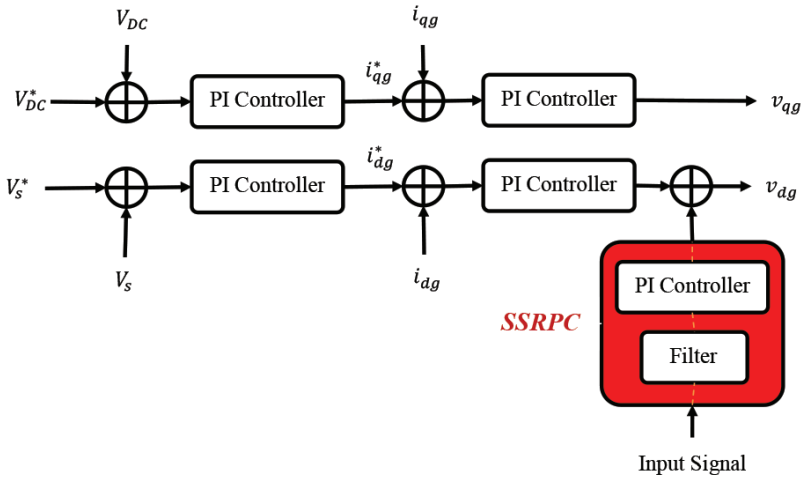

Figure 3. Connecting point of the SSRPC.

6. Case study and simulation results

The software MATLAB/Simulink and the IEEE SSR first benchmark model (Figure 1) were used. This system has fifty 2-MW DFIGs, assumed to be equivalent to a 100-MW DFIG. It is connected to an infinite bus through a capacitive series compensated transmission line, and its parameters are given elsewhere [7, 28]. The system's poles were calculated at a compensation level of 20% and a wind speed of 7 m/s using the system state matrix, shown in Table 2. As observed, modes 6 and 7 had a frequency of 36.51 Hz, which is the same as that of SSR modes. Since all relations were transformed into the qd0-frame rotating with the synchronous speed, the SSR mode frequency was equal to $f_s - f_n$. Therefore, the subsynchronous resonance frequency was 23.49 Hz. Figure 4 shows the effect of the compensation level on the SSR mode. In this figure, the poles of the system are represented by (*), and the poles of the SSR mode are displayed with (o) regarding different compensation levels. This figure shows that by increasing the compensation level the SSR mode became unstable because according to the slip relation (S_n), with the increase in the compensation level, the resonant frequency increased, and the amplitude of (S_n) became smaller. As the S_n is negative, the rotor's resistance amplitude increases, and the system moves toward instability. According to Figure 4, at a wind speed of 7 m/s, the compensation levels of 60%, 70%, and 80% for this system resulted in the instability of the SSR mode. Since the SSR in DFIG wind farms is caused by the IGE, the dynamics of the shaft, the RSC controller, and the GSC controller can be disabled to obtain the SSR mode.

Table 3 shows the participation factors of the state variables in the system deferent modes. The modes of λ_6 and λ_7 are SSR modes. According to this table, the voltage of the line series capacitor had the highest participation in SSR modes. Its participation factor is a value of 0.26. For this reason, this variable was considered as the input signal for the SSRPC. According to Figure 4, to increase the line transmission power, the maximum compensation level of this system was approximately 50% at a wind speed of 7 m/s. In the present paper, using the proposed controller, the maximum compensation level of the line significantly increased. To confirm the proposed method, it was primarily assumed that the system had a compensation level of 20% at a wind speed of 7 m/s and was stable in normal operations. At 100 s, the compensation level increased to 70%. Figure 5a shows the rotor speed oscillations due to the increase in the compensation level from 20% to 70%. According to this figure, since SSR occurred at 100 s, the system without the SSRPC was unstable.

Table 2. System poles at wind speed of 7 m/s and compensation level of 20%.

Mode number	Poles
1	0
2,3	-16.58±1210i
4,5	-7.5±514.8i
6,7	-5.77±229.4i
8	0
9,10	-5.86±94.45i
11,12	-0.5±6.14i

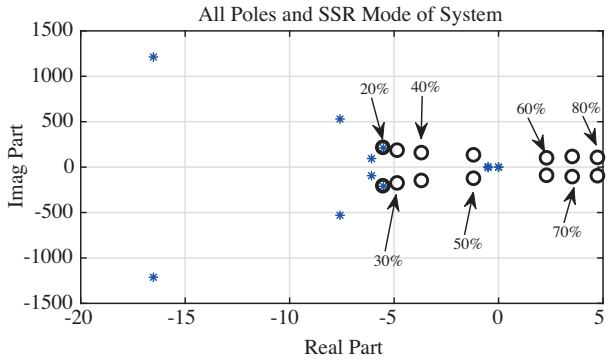

Figure 4. SSR modes and other poles at wind speed of 7 m/s and deferent compensation levels

However, using the SSRPC, the system was stable. This figure shows the SSRPC creating dynamic stability of the DFIG wind farm and providing the possibility of a high compensation level. In addition, the most important point is that the rotor speed moved back to the initial value prior to increasing the compensation (at a wind speed of 7 m/s, the reference wind speed value is 0.75). These results mean that the signal selected for the proposed controller and its applying location were correctly selected. Figure 5b presents the most important result, which is associated with the electric torque oscillations. The good results pertaining to this figure show that the SSRPC was able to damp the electrical torque oscillations and return the electrical torque to the value prior to the increase in the compensation (at a wind speed of 7 m/s, the reference torque value is 0.43). In other words, the MPPT condition was preserved for the wind speed of 7 m/s, which is of great importance. The reason for such importance is that the location to apply the SSRPC and the input signal do not directly affect MPPT parameters such as the turbine speed, power, and torque. The SSRPC only prevents the IGE through controlling the line current with the help of the stator voltage and the GSC output voltage. Figure 6a indicates electrical power oscillations that were damped using the SSRPC. In addition, Figure 6b shows the increase in the line current during the SSR occurrence caused by the IGE. The line current increased and oscillated owing to the increase in the compensation level, and the system became unstable. However, using the SSRPC, the current oscillations were damped and its increase was prevented. Therefore, the proposed controller was able to prevent the instability caused by the IGE using an effective factor in SSR mode, which is the line series capacitor voltage.

Additionally, Figure 7a shows the stator voltage oscillations. According to this figure, by applying the proposed controller to the GSC output voltage, the stator voltage oscillations were well controlled and damped.

Table 3. Participation factors of state variables on system modes.

State variable	Mode						
	λ_1	λ_2 & λ_3	λ_4 & λ_5	λ_6 & λ_7	λ_8	λ_9 & λ_{10}	λ_{11} & λ_{12}
ψ_{qs}	0	0.35	0.11	0.05	0	0.003	0
ψ_{ds}	0	0.35	0.11	0.05	0	0.003	0
ψ_{qr}	0	0.002	0.0006	0.001	0.0002	0.5	0.0006
ψ_{dr}	0	0.002	0.0006	0.001	0.0002	0.5	0.0007
ω_t	0	0	0	0	0.83	0	0.42
ω_r	0	0	0	0	0.17	0.001	0.5
T_g	0	0	0	0	0	0.0001	0
I_{qL}	0	0.15	0.16	0.2	0	0.002	0
I_{dL}	0	0.15	0.16	0.2	0	0.002	0
v_{qc}	0	0.007	0.24	0.26	0	0.0004	0
v_{dc}	0	0.007	0.24	0.26	0	0.0004	0
V_{DC}	1	0	0	0	0	0	0

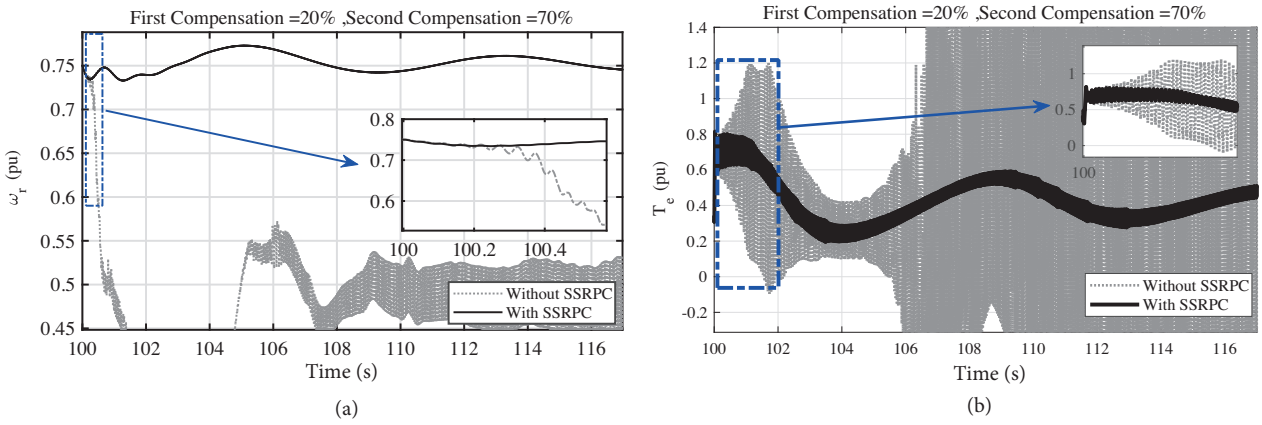

Figure 5. System oscillations at wind speed of 7 m/s and with increasing compensation level from 20% to 70%; (a) rotor speed, (b) electrical torque.

Figure 7b further indicates the DC-link capacitor voltage. According to this figure, by SSRPC, the DC-link capacitor voltage was stable and had slight oscillations.

7. Discussion

- A high level of compensation in the lines connected to DFIG-based wind farms has been the most important goal of this article. For this purpose, in critical condition with the critical wind speeds (7 m/s), 70% compensation was performed using a proposed method. The simulations and proposed methods of the articles in the literature are for compensation levels less than 65%. For example, in Mohammadpour and Santi [2], the maximum compensation level was 65%, and in Mohammadpour et al. [19], the maximum compensation level was 55%.

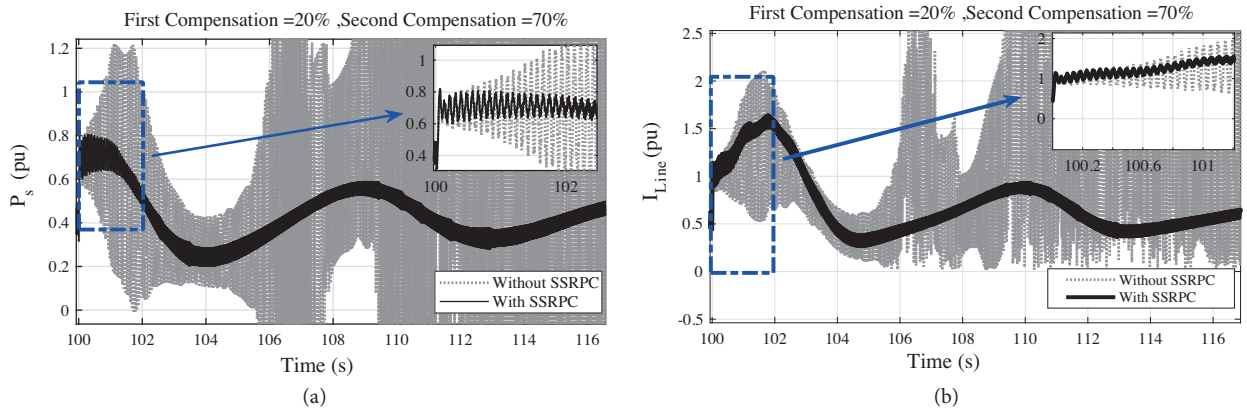

Figure 6. System oscillations at wind speed of 7 m/s and with increasing compensation level from 20% to 70%; (a) electrical power, (b) line current.

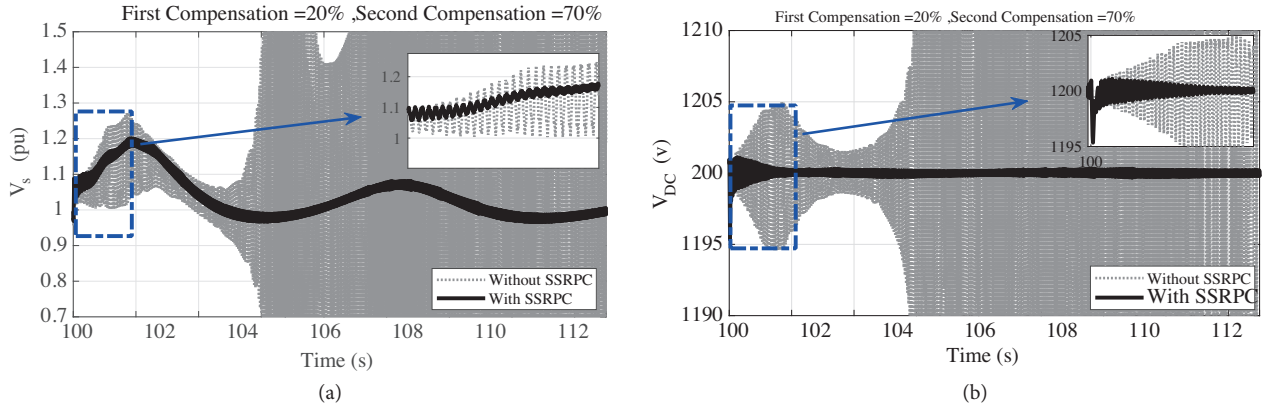

Figure 7. System oscillations at wind speed of 7 m/s and with increasing compensation level from 20% to 70%; (a) stator voltage, (b) DC-link capacitor voltage.

- Moreover, the proposed method in the present paper is simpler than other mitigation techniques and does not require complex mathematical methods. Our study did not use additional expensive devices such as FACTS devices.
- The exact and complete step-step linearization of the differential and algebraic equations is also presented in this paper.

8. Conclusion

This study provided the possibility of a high compensation level for the power transmission lines of DFIG wind farms by SSRPC. Using the analysis of the equations, an effective and logical method was proposed; this method prevented the SSR phenomenon at the high-compensation level of the transmission line. The SSRPC was proposed for application to the GSC output voltage. The objective of such a proposition is based on the direct effect on the IGE and maintenance of MPPT. In addition, based on the modal analysis and the participation factors, the input signal was introduced to the proposed controller. According to the participation factors, the series capacitor voltage of the line had the highest participation in the SSR modes. Thus, it is used

as the input signal to the proposed controller. To investigate the performance of the proposed method, the IEEE SSR first benchmark model was simulated by use of the dynamic equations in MATLAB/Simulink to which the proposed method was applied. The simulation results showed that the proposed method was correct and highly effective. According to these results, application of the SSRPC to the GSC output voltage significantly increased the capacitive series compensation level and maintained MPPT. Moreover, this method enhanced the damping and reduced the amplitude of the oscillations. Therefore, the proposed method prevented SSR instability at high compensation levels and, importantly, did not change MPPT conditions.

References

[1] Lie X, Cartwright P. Direct active and reactive power control of DFIG for wind energy generation. IEEE Transactions on Energy Conversion 2006; 21 (3): 750-758. doi: 10.1109/TEC.2006.875472

[2] Mohammadpour HA, Santi E. Optimal adaptive sub-synchronous resonance damping controller for a series-compensated doubly-fed induction generator-based wind farm. IET Renewable Power Generation 2015; 9 (6): 669-681. doi: 10.1049/iet-rpg.2014.0155

[3] Sahni M, Badrzadeh B, Muthumuni D, Cheng Y, Yin H et al. Sub-synchronous interaction in Wind Power Plants-part II: An ercot case study. In: IEEE Power and Energy Society General Meeting; San Diego, CA, USA; 2012. pp. 1-9.

[4] Sahni M, Muthumuni D, Badrzadeh B, Gole A, Kulkarni A. Advanced screening techniques for Sub-Synchronous Interaction in wind farms. In: EEE PES Transmission and Distribution Conference and Exposition (T&D); Orlando, FL, USA; 2012. pp. 1-9.

[5] Wang L, Xie X, Jiang Q, Pota HR. Mitigation of multimodal subsynchronous resonance via controlled injection of supersynchronous and subsynchronous currents. IEEE Transactions on Power Systems 2014; 29 (3): 1335-1344. doi: 10.1109/TPWRS.2013.2292597

[6] Xie H, Oliveira MMD. Mitigation of SSR in presence of wind power and series compensation by SVC. In: Power System Technology (POWERCON); Chengdu, China; 2014. pp. 2819-2826.

[7] Suriyaarachchi DHR, Annakkage UD, Karawita C, Kell D, Mendis R et al. Application of an SVC to damp sub-synchronous interaction between wind farms and series compensated transmission lines. In: IEEE Power and Energy Society General Meeting; San Diego, CA, USA; 2012. pp. 1-6.

[8] Boopathi VP, Muzamil AR, Kumudini DRP, Ramanujam R. Analysis and mitigation of subsynchronous oscillations in a radially-connected wind farm. In: Power and Energy Systems: Ttowards Sustanable Eenergy ; Bangalore, India ; 2014. pp. 1-7.

[9] Varma RK, Auddy S, Semsedini Y. Mitigation of subsynchronous resonance in a series-compensated wind farm using FACTS controllers. IEEE Transactions on Power Delivery 2008; 23 (3): 1645-1654. doi: 10.1109/TPWRD.2008.917699

[10] Mohammadpour HA, Santi E. Sub-synchronous resonance analysis in DFIG-based wind farms: mitigation methods-TCSC, GCSC, and DFIG controllers-part II. In: IEEE Energy Conversion Congress and Exposition (ECCE); Pittsburgh, PA, USA; 2014. pp. 1550-1557.

[11] Mohammadpour HA, Santi E. Modeling and control of gate-controlled series capacitor interfaced with a DFIG-based wind farm. IEEE Transactions on Industrial Electronics 2015; 62 (2): 1022-1033. doi: 10.1109/TIE.2014.2347007

[12] Mohammadpour HA, Shin YJ, Santi E. SSR analysis of a DFIG-based wind farm interfaced with a gate-controlled series capacitor. In: Twenty-Ninth Annual IEEE in Applied Power Electronics Conference and Exposition (APEC); Fort Worth, TX, USA; 2014. pp. 3110-3117.

[13] Thirumalaivasan R. Janaki MR. Xu YJ. Kalman filter based detection and mitigation of subsynchronous resonance with SSSC. IEEE Transactions on Power Systems 2017; 32 (2): 1400-1409. doi: 10.1109/TPWRS.2016.2572301

[14] Moursi MSE, Khadkikar V. Novel control strategies for SSR mitigation and damping power system oscillations in a series compensated wind park. In: 38th Annual Conference on IEEE Industrial Electronics Society in IECON; Montreal, QC, Canada; 2012, pp. 5335-5342.

[15] Abdou AF, Abu-Siada A, Pota HR. Damping of subsynchronous oscillations and improve transient stability for wind farms. In: Innovative Smart Grid Technologies Asia (ISGT); Beijing, China; 2011. pp. 1-20.

[16] Moharana A, Varma RK, R Seethapathy. SSR mitigation in wind farm connected to series compensated transmission line using STATCOM. In: IEEE Power Electronics and Machines in Wind Applications; Denver, CO, USA; 2012. pp. 1-8.

[17] Moharana A, Varma RK, Seethapathy R. SSR alleviation by STATCOM in induction-generator-based wind farm connected to series compensated line. IEEE Transactions on Sustainable Energy 2014; 5 (3): 947-957. doi: 10.1109/TSTE.2014.2311072

[18] Fan L, Miao Z. Mitigating SSR using DFIG-based wind generation. IEEE Transactions on Sustainable Energy 2012; 3 (3): 349-358. doi: 10.1109/TSTE.2012.2185962

[19] Mohammadpour HA, Ghaderi A, Mohammadpour H, Santi E. SSR damping in wind farms using observed-state feedback control of DFIG converters. Electric Power Systems Research 2015; 123: 57-66. doi: 10.1016/j.epsr.2015.01.018

[20] Zhao B, Li H, Wang M, Chen Y, Liu S et al. An active power control strategy for a DFIG-based wind farm to depress the subsynchronous resonance of a power system. International Journal of Electrical Power & Energy Systems 2015; 69: 327-334. doi: 10.1016/j.ijepes.2015.01.002

[21] Mohammadpour HA, Santi E. SSR damping controller design and optimal placement in rotor-side and grid-side converters of series-compensated DFIG-based wind farm. IEEE Transactions on Sustainable Energy 2015; 6 (2): 388-399. doi: 10.1109/TSTE.2014.2380782

[22] Zhang X, Xie X, Liu H, Liu Hui, Li Y et al. Mitigation of sub-synchronous control interaction in wind power systems with GA-SA tuned damping controller. IFAC-PapersOnLine 2017; 50 (1): 8740-8745. doi: 10.1016/j.ifacol.2017.08.1730

[23] Wang Y, Wu Q, Yang R, Tao G, Liu Z et al. H∞ current damping control of DFIG based wind farm for subsynchronous control interaction mitigation. International Journal of Electrical Power & Energy Systems 2018; 98: 509-519. doi: 10.1016/j.ijepes.2017.12.003

[24] Liu H, Xie X, Li Y, Liu H, Hu Y. Mitigation of SSR by embedding subsynchronous notch filters into DFIG converter controllers. IET Generation, Transmission & Distribution 2017; 11 (11): 2888-2896. doi: 10.1049/iet-gtd.2017.0138

[25] Liu H, Xie X, Zhang C, Li Y, Liu H et al. Quantitative SSR analysis of series-compensated DFIG-based wind farms using aggregated RLC circuit model. IEEE Transactions on Power Systems 2017; 32 (1): 474-483. doi: 10.1109/TPWRS.2016.2558840

[26] Xie X, Zhang X, Liu H, Liu Hui, Li Y et al. Characteristic analysis of subsynchronous resonance in practical wind farms connected to series-compensated transmissions. IEEE Transactions on Energy Conversion 2017; 32 (3): 1117-1126. doi: 10.1109/TEC.2017.2676024

[27] Song Y, Blaabjerg F. Overview of DFIG-based wind power system resonances under weak networks. IEEE Transactions on Power Electronics 2017; 32 (6): 4370-4394. doi: 10.1109/TPEL.2016.2601643

[28] Song Y, Wang X, Blaabjerg F. Impedance-based high-frequency resonance analysis of DFIG system in weak grids. IEEE Transactions on Power Electronics 2017; 32 (5): 3536-3548. doi: 10.1109/TPEL.2016.2584118

[29] Chen W, Xie X, Wang D, Liu H, Liu Hui. Probabilistic stability analysis of subsynchronous resonance for series-compensated DFIG-based wind farms. IEEE Transactions on Sustainable Energy 2018; 9 (1): 400-409. doi: 10.1109/TSTE.2017.2737599

[30] Xie H, Li B, Heyman C, Oliviera MMD, Monge M. Subsynchronous resonance characteristics in presence of doubly-fed induction generator and series compensation and mitigation of subsynchronous resonance by proper control of series capacitor. IET Renewable Power Generation 2014; 8 (4): 411-421. doi: 10.1049/iet-rpg.2013.0215

[31] Padiyar KR. Power System Dynamics Stability and Control. Hyderabad, India: BS Publications, 2011.

[32] Padiyar KR. Analysis of Subsynchronous Resonance in Power System. Boston, MA, USA: Kluwer Academic Publishers, 1999.

[33] Irwin GD. Jindal AK, Isaacs AL. Sub-synchronous control interactions between type 3 wind turbines and series compensated AC transmission systems. IEEE Power and Energy Society General Meeting; Detroit, MI, USA; 2011. pp. 1-6.

[34] Daniel J, Han C, Hutchinson S, Koessler S, Martin D et al. ERCOT CREZ Reactive Power Compensation Study. Zurich, Switzerland: ABB Inc., 2010.

[35] Narendra K, Fedirchuk D, Midence R, Zhang N, Mulawarman A et al. New microprocessor based relay to monitor and protect power systems against sub-harmonics. In: IEEE Electrical Power and Energy Conference; Winnipeg, MB, Canada; 2011. pp. 438-443.

[36] Reader's guide to subsynchronous resonance. IEEE Transactions on Power Systems 1992; 7 (1): 150-157.

[37] Bongiorno M, Petersson A. The Impact of Wind Farms on Subsychronous Resonance in Power Systems, Elforsk rapport 11:29. Stockholm, Sweden: Elforsk AB, 2011.

[38] Piwko R, Miller N, Sanchez-Gasca J, Yuan X, Dai R et al. Integrating Large Wind Farms into Weak Power Grids with Long Transmission Lines. In: IEEE/PES Transmission & Distribution Conference & Exposition: Asia and Pacific; Dalian, China; 2005. pp. 1-7.

[39] Miller NW, Sanchez-Gasca JJ, Price WW, Delmerico RW. Dynamic modeling of GE 1.5 and 3.6 MW wind turbine-generators for stability simulations. In: IEEE Power Engineering Society General Meeting; Toronto, ON, Canada; 2003. pp. 1977-1983.

[40] Bialasiewicz JT, Muljadi E. The Wind Farm Aggregation Impact on Power Quality. In: IECON 2006 - 32nd Annual Conference on IEEE Industrial Electronics; Paris, France; 2006. pp. 4195-4200.

[41] Fernandez LM, Jurado F, Saenz JR. Aggregated dynamic model for wind farms with doubly fed induction generator wind turbines. Renewable Energy 2008; 33 (1): 129-140. doi: 10.1016/j.renene.2007.01.010

[42] Fan L, Kavasseri R, Miao Z, Zhu C. Modeling of DFIG-based wind farms for SSR analysis. IEEE Transactions on Power Delivery 2010; 25 (4): 2073-2082. doi: 10.1109/TPWRD.2010.2050912

[43] Krause PC, Wasynczuk O, Sudhoff SD. Analysis of electric machinery. Piscataway, NJ, USA: IEEE Press, 1995.

[44] Pulgar-Painemal HA. Wind farm model for power system stability analysis. PhD. University of Illinois at Urbana-Champaign, Urbana, IL, USA, 2010.

[45] Mei F, Pal BC. Modelling of dobuly-fed induction generator for power system stability study. In: IEEE Power and Energy Society General Meeting - Conversion and Delivery of Electrical Energy in the 21st Century; Pittsburgh, PA, USA; 2008. pp. 1-8.

[46] Fan L, Zhu C, Miao Z, Hu M. Modal analysis of a DFIG-based wind farm interfaced with a series compensated network. IEEE Transactions on Energy Conversion 2011; 26 (4): 1010-1020. doi: 10.1109/TEC.2011.2160995

[47] Gahramani H, Lak A, Farsadi M, Hosseini H. Mitigation of SSR and LFO with a TCSC based-conventional damping controller optimized by the PSO algorithm and a fuzzy logic controller. Turkish Journal of Electrical Engineering & Computer Sciences 2013; 21: 1302-1317. doi: 10.3906/elk-1112-81

[48] Motiebirjandi AA, Fateh D. Optimal placement method of multi UPFCs to damp power system oscillations. International Transactions on Electrical Energy Systems 2017; 27 (9): 1-13. doi: 10.1002/etep.2360

[49] Kundur P. Power System Stability and Control. Michigan, USA: Mc Graw Hill, 1994.